Copyrights IEEE 2013

Cascaded VFO set-point control for N-trailers with on-axle hitching

Maciej Michałek, *Member, IEEE*, Marcin Kiełczewski,

***Abstract*—Set-point control task for N-trailers corresponds to the practical problem of parking/docking maneuvers performed by a vehicle comprising of an active tractor and N passively interconnected trailers. So far, solutions to the automated parking problem for N-trailers have been formulated mostly by using highly nonlinear local transformations of vehicle kinematics into the chained form. Inherent limitations of this approach motivated the authors to propose an alternative cascaded control solution with the Vector-Field-Orientation (VFO) controller used in the outer loop. The new control law proposed in the paper does not involve any auxiliary model transformation and is highly scalable. The concept has been verified by simulations and by results of experimental trials conducted with a 3-trailer vehicle.**

***Index Terms*—N-trailer, on-axle hitching, cascaded control**

I. Introduction

Kinematics of N-trailer vehicles (N-trailers) combine several specific properties like high nonlinearity, nonholonomy, structural singularity, and in-joint instability making the control problems for N-trailers especially difficult. This fact may explain a considerable interest taken by the control community in the N-trailers and related control problems, see e.g. [5], [24], [25], [34], [36]. One may distinguish three types of N-trailer structures. Depending on the number $M \in [0, N]$ of off-axle interconnections applied between vehicle segments one can say about *standard N-trailers* (SNT) if $M = 0$, [13], [16], [30], *non-standard N-trailers* (nSNT) if $M = N$, [9], or *general N-trailers* (GNT) if $0 < M < N$, [1], [19]. Every type of N-trailer is characterized by specific control-relevant properties [1], [10], [30]. However, some structural properties common for all the N-trailers exclude the existence of any smooth asymptotically stabilizing time-invariant state-feedback for this kind of systems in the case of constant reference configurations (necessary Brockett's conditions are violated [7]). It makes the set-point control task particularly difficult despite its fairly simple definition.

In this brief we focus on the set-point control problem for SNT kinematics which belong to differentially flat systems [30], and can be locally transformable into the chained form [27], [35]. The latter property has been widely utilized in the literature due to availability of numerous control strategies for chained systems [2], [14], [32]. Examples of control solutions for N-trailers based on the chained-form transformation can be found in [23], [24], [28], [31], [35]. This undoubtedly general and elegant approach has however some inherent limitations. They result from application of highly nonlinear local transformations of the original configuration variables and control inputs, which essentially constrain admissible configurations of the vehicle. The widely used transformation proposed in [27] makes the transformed model valid only if the orientation of a last trailer and the joint angles are all confined to the range $(-\frac{\pi}{2}; \frac{\pi}{2})$. As indicated in [21], ill-conditioning of highly nonlinear transformations may make the resultant controller extremely sensitive to small changes of configuration variables implying substantial deterioration of control performance in the original (task) space. Furthermore, the chained-form approach may lead to very complex resultant controllers, especially if a number of trailers is large [23], [26]. This in turn may cause serious problems with proper tuning of the controllers to ensure practically acceptable vehicle motion in a task space [21].

To avoid the limitations of the chained-form approach we propose an alternative cascaded control concept, which does not require any auxiliary transformation of the SNT model. In the proposed approach a control system consists of an outer loop dedicated to a posture of the last trailer, and N inner loops closed around particular vehicle joints. In the outer loop we apply the Vector-Field-Orientation (VFO) control strategy, which proved especially efficient for unicycle-like kinematics [11]. The cascaded control structure is highly scalable and can be instantly applied to vehicles with different numbers of trailers. The brief is a substantial extension of work [8].

Authors are with Chair of Control and Systems Engineering, Poznań University of Technology, Piotrowo 3a, 60-965 Poznań, Poland, e-mail: maciej.michalek/marcin.kielczewski@put.poznan.pl

II. Vehicle kinematics and problem statement

Fig. 1 presents a kinematic skeleton of a standard N-trailer. It consists of an active tractor and N trailers of lengths $L_i > 0$, $i = 1, \ldots, N$. Trailers are interconnected in a chain by the passive rotary joints of on-axle type. The vehicle configuration

$$\boldsymbol{q} \triangleq [\boldsymbol{\beta}^\top \ \bar{\boldsymbol{q}}^\top]^\top = [\beta_1 \ \ldots \ \beta_N \ \theta_N \ x_N \ y_N]^\top \in \mathbb{R}^{N+3}, \quad (1)$$

consists of the joint-angle vector $\boldsymbol{\beta} \in \mathbb{R}^N$, and the last-trailer posture vector $\bar{\boldsymbol{q}} \in \mathbb{R}^3$ (cf. Fig. 1). Point $P = (x_N, y_N)$, with coordinates being the flat outputs of SNT kinematics [18], [30], will be called the *guidance point* of a vehicle. As a consequence, the last trailer will be called the *guidance segment*. The vehicle control input $\boldsymbol{u}_0 = [\omega_0 \ v_0]^\top \in \mathbb{R}^2$ consists of the angular and longitudinal velocities of the tractor, respectively.

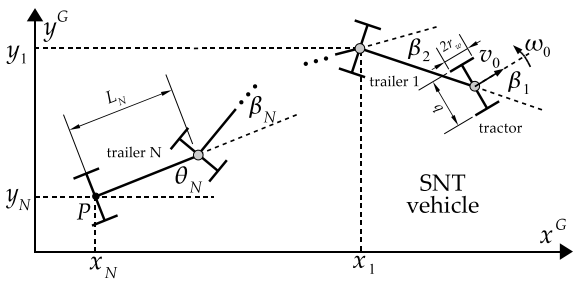

Fig. 1. Kinematic skeleton of SNT vehicle in a global frame $\{x^G, y^G\}$

Assuming the rolling-without-slipping condition, kinematics of every i-th segment can be treated as the unicycle

$$\dot{\theta}_i = \omega_i, \quad \dot{x}_i = v_i \cos\theta_i, \quad \dot{y}_i = v_i \sin\theta_i, \tag{2}$$

where ω_i and v_i are the angular and longitudinal velocities of the i-th segment, respectively (cf. Fig. 1). Velocities ω_i and v_i satisfy the following propagation formula

$$\begin{bmatrix}\omega_i \\ v_i\end{bmatrix} = \boldsymbol{J}_i(\beta_i)\begin{bmatrix}\omega_{i-1} \\ v_{i-1}\end{bmatrix}, \quad \boldsymbol{J}_i(\beta_i) = \begin{bmatrix}0 & \frac{1}{L_i}\sin\beta_i \\ 0 & \cos\beta_i\end{bmatrix}, \tag{3}$$

$i = 1, \ldots, N$, where the i-th joint angle

$$\beta_i = \theta_{i-1} - \theta_i. \tag{4}$$

Relations (3)-(4) describe how tractor inputs ω_0 and v_0 propagate to the i-th trailer along the vehicle kinematic chain. Using equations (2)-(4) one may formulate kinematics of the SNT vehicle in a cascaded form [9] or in a form of driftless system

$$\dot{\boldsymbol{q}} = \boldsymbol{S}(\boldsymbol{q})\boldsymbol{u}_0 \tag{5}$$

with the appropriate kinematic matrix $\boldsymbol{S}(\boldsymbol{q})$ (cf. [9], [13]).

Define a reference posture for the guidance segment

$$\bar{\boldsymbol{q}}_r = [\theta_{Nr}\ x_{Nr}\ y_{Nr}]^\top \in (-\pi, \pi] \times \mathbb{R}^2, \tag{6}$$

and the posture error

$$\bar{\boldsymbol{e}} = \begin{bmatrix}e_\theta \\ e_x \\ e_y\end{bmatrix} \triangleq \begin{bmatrix}\mathcal{F}(\theta_{Nr} - \theta_N) \\ x_{Nr} - x_N \\ y_{Nr} - y_N\end{bmatrix} \in (-\pi, \pi] \times \mathbb{R}^2, \tag{7}$$

where $\mathcal{F} : \mathbb{R} \mapsto (-\pi, \pi]$.

Problem 1 (Control problem): Assume that configuration (1) is measurable, and parameters L_i are known. The objective is to design a feedback control law $\boldsymbol{u}_0 = \boldsymbol{u}_0(\bar{\boldsymbol{e}}, \boldsymbol{\beta}, \cdot)$ which ensures boundedness $\|\boldsymbol{\beta}(t)\| < \infty$ for all $t \geq 0$, and asymptotic stability of error (7) at $\bar{\boldsymbol{e}} = \boldsymbol{0}$ entailing terminal convergence of the vehicle joint angles in the sense:

$$\lim_{t\to\infty} \|\bar{\boldsymbol{e}}(t)\| = 0 \quad \Rightarrow \quad \boldsymbol{\beta}(t) \overset{t\to\infty}{\longrightarrow} \boldsymbol{0}. \tag{8}$$

The control problem emphasizes asymptotic stabilization of the guidance segment at a reference posture, while the terminal straightening of the vehicle chain is treated only as a consequence of the former. Such a formulation is less stringent when compared to a more classical approach where one expects asymptotic stabilization of all the configuration variables (1). Consequences of this fact will be commented on in Section VI-A.

III. Cascaded control strategy

A. Derivation of the cascaded control law

Assume first that there exist control functions $\Phi_\omega(\bar{\boldsymbol{e}})$, $\Phi_v(\bar{\boldsymbol{e}})$ which guarantee asymptotic stability of error (7) at zero if they could be directly applied into last-trailer kinematics (2) by taking $\omega_N := \Phi_\omega(\bar{\boldsymbol{e}})$ and $v_N := \Phi_v(\bar{\boldsymbol{e}})$ (see Section III-B).

Denoting by ω_{id}, v_{id}, and β_{id} the desired velocities and the desired joint angle for the i-th segment, respectively, the following definitions can be inferred from equation (3):

$$v_{i-1d} \triangleq L_i\omega_{id}\sin\beta_i + v_{id}\cos\beta_i, \tag{9}$$

$$\beta_{id} \triangleq \text{Atan2c}\,(L_i\omega_{id} \cdot v_{i-1d}, v_{id} \cdot v_{i-1d}) \in \mathbb{R}, \tag{10}$$

where $\text{Atan2c}\,(\cdot,\cdot) : \mathbb{R}\times\mathbb{R} \mapsto \mathbb{R}$ is a continuous version of the four-quadrant function $\text{Atan2}\,(\cdot,\cdot) : \mathbb{R}\times\mathbb{R} \mapsto (-\pi, \pi]$, introduced here to ensure continuity of β_{id} variable[1]. A sign of term v_{i-1d} in (10) determines quadrants in which β_{id} resides. Since it is not possible to force the desired angle (10) directly, let us introduce the auxiliary joint-angle error

$$e_{id} \triangleq (\beta_{id} - \beta_i) \in \mathbb{R}, \tag{11}$$

which should be made convergent to zero by the appropriately chosen velocity ω_{i-1d}. To this aim, utilize

$$\dot{\beta}_i \overset{(4)}{=} \omega_{i-1} - \omega_i =: \nu_i, \tag{12}$$

and select $\nu_i \triangleq k_i e_{id} + \dot{\beta}_{id}$ with the design parameter $k_i > 0$, and treating $\dot{\beta}_{id} \equiv d\beta_{id}/dt$ as a feed-forward term. Applying definition for ν_i into (12) results in

$$\omega_{i-1d} \triangleq \nu_i + \omega_{id} = k_i e_{id} + \dot{\beta}_{id} + \omega_{id}. \tag{13}$$

Definitions (9)-(10) and (13) constitute the so-called i-th Joint Control Module (JCM$_i$), cf. Fig. 2, with velocity input $\boldsymbol{u}_{id} = [\omega_{id}\ v_{id}]^\top$, feedback from β_i, and velocity output $\boldsymbol{u}_{i-1d} = [\omega_{i-1d}\ v_{i-1d}]^\top$. Series connection of JCM$_i$ for $i = N, \ldots, 1$ allows propagating desired velocities of the guidance segment $\omega_{Nd} := \Phi_\omega(\bar{\boldsymbol{e}})$, $v_{Nd} := \Phi_v(\bar{\boldsymbol{e}})$ to obtain desired tractor velocities ω_{0d}, v_{0d}, which in turn can be directly applied into (5) by taking $\omega_0 := \omega_{0d}$, and $v_0 := v_{0d}$. Computations can be summarized by the three-step algorithm:

S1: computation of the desired velocities for the last-trailer:

$$\omega_{Nd}(t) := \Phi_\omega(\bar{\boldsymbol{e}}(t)), \quad v_{Nd}(t) := \Phi_v(\bar{\boldsymbol{e}}(t)), \tag{14}$$

S2: propagation of the desired velocities: for $i = N$ to 1 do

$$v_{i-1d}(t) = L_i\omega_{id}(t)\sin\beta_i(t) + v_{id}(t)\cos\beta_i(t), \tag{15}$$

$$a_y(t) := L_i\omega_{id}(t)\, v_{i-1d}(t), \tag{16}$$

$$a_x(t) := v_{id}(t)\, v_{i-1d}(t), \tag{17}$$

$$\beta_{id}(t) = \text{Atan2c}\,(a_y(t), a_x(t)) \in \mathbb{R}, \tag{18}$$

$$\omega_{i-1d}(t) = k_i e_{id}(t) + \dot{\beta}_{id}(t) + \omega_{id}(t), \tag{19}$$

S3: determination of the current tractor control inputs:

$$\omega_0(t) := \omega_{0d}(t), \quad v_0(t) := v_{0d}(t). \tag{20}$$

Remark 1: The right-hand side of (18) and time-derivative $\dot{\beta}_{id}$ in (19) become undetermined for time instants $\bar{t}$ when $a_x^2(\bar{t}) + a_y^2(\bar{t}) = 0$. In this case one can formally complement definition (18) by taking $\beta_{id}(\bar{t}) := \beta_{id}(\bar{t}_-)$ where $\beta_{id}(\bar{t}_-) = \text{Atan2c}\,(a_y(\bar{t}_-), a_x(\bar{t}_-))$ with $\bar{t}_-$ directly preceding $\bar{t}$. As a consequence, one can take $\dot{\beta}_{id}(\bar{t}) := 0$.

Serially connected JCM$_i$ blocks constitute N nested inner control loops with feedbacks from angles β_i. The inputs to the N-th loop are feedback functions $\Phi_\omega(\bar{\boldsymbol{e}}(t))$ and $\Phi_v(\bar{\boldsymbol{e}}(t))$ which have to be computed on-line by an outer-loop controller. The latter will be defined in the next section by the VFO control law. A scheme in Fig. 2 explains the proposed cascaded control structure[2].

[1]For computational details of function $\text{Atan2c}\,(\cdot,\cdot)$ see Appendix A.

[2]General definitions and tools devised for stability analysis of cascaded systems can be found in [6] and references therein.

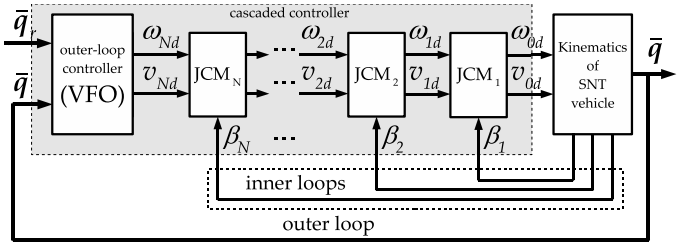

Fig. 2. Block scheme of the proposed cascaded control system

B. Description of the outer-loop VFO controller

Properties of the VFO control law allow one to obtain non-oscillatory motion of a guidance segment; they are also helpful in ensuring a self-aligning terminal behavior of a vehicle chain. Detailed description of the VFO controller can be found in [11], thus we only briefly recall equations of the VFO method.

The VFO controller formulated for unicycle kinematics (2) with $i = N$ can be described as follows:

$$\boldsymbol{\Phi}(\bar{\boldsymbol{e}}) = \begin{bmatrix} \Phi_\omega(\bar{\boldsymbol{e}}) \\ \Phi_v(\bar{\boldsymbol{e}}) \end{bmatrix} \triangleq \begin{bmatrix} k_a(\theta_a - \theta_N) + \dot{\theta}_a \\ h_x \cos\theta_N + h_y \sin\theta_N \end{bmatrix}, \tag{21}$$

where:

$$h_x = k_p e_x - \eta\sigma\sqrt{e_x^2 + e_y^2}\cos\theta_{Nr}, \tag{22}$$

$$h_y = k_p e_y - \eta\sigma\sqrt{e_x^2 + e_y^2}\sin\theta_{Nr}, \tag{23}$$

$$\theta_a = \begin{cases} \text{Atan2c}\,(\sigma\cdot h_y, \sigma\cdot h_x) & \text{for} \quad h_x^2 + h_y^2 \neq 0 \\ \theta_{Nr} \mod 2\pi & \text{for} \quad h_x^2 + h_y^2 = 0 \end{cases}, \tag{24}$$

$$\dot{\theta}_a = \begin{cases} \frac{\dot{h}_y h_x - h_y \dot{h}_x}{h_x^2 + h_y^2} & \text{for} \quad h_x^2 + h_y^2 \neq 0 \\ 0 & \text{for} \quad h_x^2 + h_y^2 = 0 \end{cases}. \tag{25}$$

In the above equations $k_a, k_p > 0$ and $\eta \in (0, k_p)$ are the design parameters, while $\sigma \in \{-1, +1\}$ is a decision factor which determines desired motion strategy for the guidance segment: forward if $\sigma := +1$ or backward if $\sigma := -1$. Decision factor σ can be almost freely selected by a designer according to the application needs. However, only selection

$$\sigma := \text{sgn}(e_x(0)\cos\theta_{Nr} + e_y(0)\sin\theta_{Nr}) \in \{-1, +1\} \tag{26}$$

ensures asymptotic convergence of error $\bar{\boldsymbol{e}}(t)$ for arbitrary initial conditions of the last trailer (cf. [9]). The sign function used in (26) is calculated upon a constant argument, thus σ does not change a value during a control process.

The form of VFO control law (21)-(25) has a clear interpretation due to inherent geometrical origins of the VFO method (see [11]). Thanks to definitions (22)-(23) one observes the characteristic *directing effect* which makes the unicycle approach a reference posture in a way resembling the garage-docking maneuvers. Intensity of this effect may be adjusted by selecting a value of η parameter (cf. Remark 3).

Let us recall what can be expected after direct application of (21) into kinematics of the last trailer (cf. [11]).

Lemma 1: Application of the VFO controller (21)-(26) into kinematics (2) for $i = N$ yields the closed-loop dynamics

$$\dot{\bar{\boldsymbol{q}}} = \bar{\boldsymbol{G}}(\bar{\boldsymbol{q}})\boldsymbol{\Phi}(\bar{\boldsymbol{e}}), \quad \bar{\boldsymbol{G}}(\bar{\boldsymbol{q}}) = \begin{bmatrix} 1 & 0 \\ 0 & \cos\theta_N \\ 0 & \sin\theta_N \end{bmatrix}, \tag{27}$$

which guarantee:

G1: $\sup_t |\Phi_\omega(\bar{\boldsymbol{e}}(t))| < \infty$, $\sup_t |\Phi_v(\bar{\boldsymbol{e}}(t))| < \infty$,
G2: $\Phi_\omega(\bar{\boldsymbol{e}}), \Phi_v(\bar{\boldsymbol{e}}) \to 0$ only if $\|\bar{\boldsymbol{e}}\| \to 0$,
G3: $\sup_t \|\bar{\boldsymbol{e}}(t)\| < \infty$ and $\lim_{t\to\infty} \|\bar{\boldsymbol{e}}(t)\| = 0$

for any bounded initial posture error $\bar{\boldsymbol{e}}(0) \in (-\pi, \pi] \times \mathbb{R}^2$.

Definitions (21)-(26) formally make $\bar{\boldsymbol{e}} = \boldsymbol{0}$ an equilibrium of dynamics (27), thus G3 implies asymptotic stability of $\bar{\boldsymbol{e}} = \boldsymbol{0}$ in the Lyapunov sense.

C. Main proposition

Proposition 1: Let ϵ be some non-negative vicinity prescribed by a designer. Assume what follows:

A1. $\forall\, t \geq 0 \;\; |\beta_{id}(t)| < \frac{\pi}{2}$ for $i = 1, \ldots, N$,
A2. $\forall\, i \;\; |\beta_i(0)| < \frac{\pi}{2}$ and $\bar{\boldsymbol{e}}(0) \in (-\pi, \pi] \times (\mathbb{R}^2 \setminus \mathcal{B}_r)$ with zero-centered ball $\mathcal{B}_r$ of sufficiently large radius $r > \epsilon$.

Under assumptions A1-A2 control law (14)-(20) with $k_i > 0$ satisfying (54), and with outer-loop VFO controller (21)-(26), applied into SNT kinematics (5) in a way that

$$\boldsymbol{u}_0 = \begin{bmatrix} \omega_0 \\ v_0 \end{bmatrix} := \begin{cases} \begin{bmatrix} \omega_{0d} & v_{0d} \end{bmatrix}^\top & \text{for} \quad \left\| \bar{\boldsymbol{W}}\bar{\boldsymbol{e}} \right\| > \epsilon \\ \begin{bmatrix} 0 & 0 \end{bmatrix}^\top & \text{for} \quad \left\| \bar{\boldsymbol{W}}\bar{\boldsymbol{e}} \right\| \leq \epsilon \end{cases}, \tag{28}$$

where $\bar{\boldsymbol{W}} \triangleq \text{diag}\{w_\theta, 1, 1\}$, $w_\theta \in (0, 1]$ is a weighting matrix,

i) solves Problem 1 if $\epsilon = 0$,
ii) approximately solves Problem 1 if $\epsilon > 0$ in the sense: $\forall\, \epsilon > 0\; \exists T < \infty$ and $\exists\, \delta = \delta(\epsilon, \bar{\boldsymbol{e}}(0), \boldsymbol{\beta}(0), k_p - \eta)$ such that $\forall\, t \geq T \;\; \left\| \bar{\boldsymbol{W}}\bar{\boldsymbol{e}}(t) \right\| \leq \epsilon, \;\; \|\boldsymbol{\beta}(t)\| \leq \delta$.

Assumption A1 has been introduced mainly for purposes of the proof presented in Section III-D (see also Remark 2). Assumption A2 is not very limiting in practice, since application of the preliminary open-loop control $\boldsymbol{u}_0 := [0 \;\; V]^\top$, $V > 0$ ensures satisfaction of A2 in finite time. Note that (28) determines the vehicle stopping condition activated when the weighted posture error enters the prescribed vicinity ϵ.

D. Proof of Proposition 1

Detailed analysis will be done for the *nominal* case with $\epsilon = 0$. Analysis for the approximate case with $\epsilon > 0$ will be a consequence of the former.

First, consider the inner-loops dynamics by showing boundedness and convergence of the auxiliary joint-angle error

$$\boldsymbol{e}_d = \begin{bmatrix} e_{1d} \\ \vdots \\ e_{Nd} \end{bmatrix} \triangleq \begin{bmatrix} \beta_{1d} - \beta_1 \\ \vdots \\ \beta_{Nd} - \beta_N \end{bmatrix} \in \mathbb{R}^N. \tag{29}$$

Lemma 2: Dynamics of error (29) take the form

$$\dot{\boldsymbol{e}}_d = -\boldsymbol{A}\boldsymbol{e}_d + \boldsymbol{\Gamma}\sin\boldsymbol{e}_d, \tag{30}$$

where $\boldsymbol{A} = \text{diag}\{k_i\}$, $k_i > 0$, $i = 1, \ldots, N$, are the gains introduced in (19), and $\boldsymbol{\Gamma}_{N\times N}$ is the lower-triangular matrix such that $\|\boldsymbol{\Gamma}\| \leq g < \infty$. Solution of equation (30) is uniformly bounded in time and

$$\forall\, t \geq 0 \quad \|\boldsymbol{e}_d(t)\| \leq \|\boldsymbol{e}_d(0)\| \exp(-(1-\rho)\underline{k}t) \tag{31}$$

if k_i are such that: $\underline{k} \triangleq \min_i\{k_i\} \geq g/\rho$ for $\rho \in (0, 1)$.

Proof: See Appendix C-0a. ■

From now on, we assume that gains k_i are selected according to the above suggestion guaranteeing (31).

Second, let us analyze closed-loop behavior of posture error (7). Assume for simplicity (and without loss of generality) that $\bar{\boldsymbol{q}}_r = \mathbf{0}$. Since $\dot{\bar{\boldsymbol{e}}} = -\dot{\bar{\boldsymbol{q}}}$ and $\bar{\boldsymbol{G}}(\bar{\boldsymbol{q}}) = \bar{\boldsymbol{G}}(-\bar{\boldsymbol{e}})$, one can rewrite kinematics (2) for $i = N$ as $\dot{\bar{\boldsymbol{e}}} = -\bar{\boldsymbol{G}}(-\bar{\boldsymbol{e}})\boldsymbol{u}_N$, where $\bar{\boldsymbol{G}}(-\bar{\boldsymbol{e}})$ results from (27), and $\boldsymbol{u}_N = [\omega_N \; v_N]^\top$. By recalling (14) the input $\boldsymbol{u}_N$ can be expressed as $\boldsymbol{u}_N = \boldsymbol{\Phi}(\bar{\boldsymbol{e}}) - \boldsymbol{e}_{\omega vN}$ where

$$\boldsymbol{e}_{\omega vN} = \begin{bmatrix} \omega_{Nd} - \omega_N \\ v_{Nd} - v_N \end{bmatrix} = \underbrace{\begin{bmatrix} 0 & \dots & 1 & 0 & \dots & 0 \\ 0 & \dots & 0 & 0 & \dots & 1 \end{bmatrix}}_{\boldsymbol{L}_{2\times 2N}} \boldsymbol{e}_{\omega v} \quad (32)$$

with $\boldsymbol{e}_{\omega v}$ defined in (45). Now, posture error dynamics can be formulated as $\dot{\bar{\boldsymbol{e}}} = \boldsymbol{f}_n(\bar{\boldsymbol{e}}) + \boldsymbol{g}(\bar{\boldsymbol{e}}, \boldsymbol{e}_{\omega v}) = \boldsymbol{f}(\bar{\boldsymbol{e}}, \boldsymbol{e}_{\omega v})$, where $\boldsymbol{f}_n(\bar{\boldsymbol{e}}) = -\bar{\boldsymbol{G}}(-\bar{\boldsymbol{e}})\boldsymbol{\Phi}(\bar{\boldsymbol{e}})$ and $\boldsymbol{g}(\bar{\boldsymbol{e}}, \boldsymbol{e}_{\omega v}) = \bar{\boldsymbol{G}}(-\bar{\boldsymbol{e}})\boldsymbol{L}\boldsymbol{e}_{\omega v}$. It can be shown (see Appendix C-0b) that $\boldsymbol{e}_{\omega v} = \boldsymbol{H}\sin\boldsymbol{e}_d$ with $\sin\boldsymbol{e}_d(t) = [\sin e_{1d} \; \dots \; \sin e_{Nd}]^\top \in [-1, 1]^N$ and some bounded matrix $\boldsymbol{H}_{2N\times N}$. As a consequence

$$\dot{\bar{\boldsymbol{e}}} = \boldsymbol{f}_n(\bar{\boldsymbol{e}}) + \boldsymbol{g}(\bar{\boldsymbol{e}}, \boldsymbol{e}_d) = \boldsymbol{f}(\bar{\boldsymbol{e}}, \boldsymbol{e}_d), \quad (33)$$

with perturbing term $\boldsymbol{g}(\bar{\boldsymbol{e}}, \boldsymbol{e}_d) = \bar{\boldsymbol{G}}(-\bar{\boldsymbol{e}})\boldsymbol{L}\boldsymbol{H}\sin\boldsymbol{e}_d$ such that $\boldsymbol{g}(\bar{\boldsymbol{e}}, \mathbf{0}) = \mathbf{0}$. Hence, (33) can be treated as a system with state $\bar{\boldsymbol{e}}$ and perturbing input $\boldsymbol{e}_d$, where $\dot{\bar{\boldsymbol{e}}} = \boldsymbol{f}_n(\bar{\boldsymbol{e}}) = \boldsymbol{f}(\bar{\boldsymbol{e}}, \mathbf{0})$ represents the zero-input dynamics of (33). According to (31), the perturbing term $\boldsymbol{g}(\bar{\boldsymbol{e}}, \boldsymbol{e}_d)$ vanishes in time. The following lemma states the input-to-state stability (ISS) of (33).

Lemma 3: System (33) has a uniformly bounded solution $\bar{\boldsymbol{e}}(t)$ and is ISS with respect to input $\boldsymbol{e}_d$.

Proof: See Appendix C-0b. ■

Combining (33) with (30) gives the cascaded system having the following properties: 1° both $\dot{\bar{\boldsymbol{e}}} = \boldsymbol{f}(\bar{\boldsymbol{e}}, \mathbf{0})$ and (30) have globally asymptotically stable equilibria $\bar{\boldsymbol{e}} = \mathbf{0}$ and $\boldsymbol{e}_d = \mathbf{0}$, respectively (cf. Lemma 1 and (31)), 2° the *driven* system (33) is ISS with respect to input $\boldsymbol{e}_d$. Now, by application of Lemma 4.7 included in [15], one claims asymptotic stability of point $(\bar{\boldsymbol{e}}, \boldsymbol{e}_d) = (\mathbf{0}, \mathbf{0})$ in the cascaded system.

Finally, let us analyze boundedness and terminal convergence of joint angles β_i. Upon assumption A1 and due to (31) one concludes boundedness of joint-angles β_i. In order to show the terminal behavior of angles β_i it suffices to reveal the terminal convergence of desired angles $\beta_{id}(t)$ as $t \to \infty$.

Lemma 4: In the case where $\epsilon = 0$ holds

$$\beta_{id}(t) \to 0 \quad \text{as} \quad t \to \infty, \quad i = 1, \dots, N. \quad (34)$$

Proof: See Appendix C-0c ■

Combination of (31) with (34) implies terminal convergence of joint angles: $\beta_i(t) \to 0$ as $t \to \infty$ for $i = 1, \dots, N$.

Let us consider consequences of selection $\epsilon > 0$ in condition (28). The second row of (28) determines the vehicle stopping condition, since application $\boldsymbol{u}_0 := \mathbf{0}$ into (5) instantaneously freezes all the configuration variables. If the weighted posture error is outside vicinity ϵ, then all the conclusions related to boundedness and convergence tendency are preserved like in the nominal case for $\epsilon = 0$. Since in the nominal case posture error $\bar{\boldsymbol{e}}(t)$ tend to zero in infinite time, thus for $\epsilon > 0$ there exists finite time instant $T = T(\epsilon, \cdot)$ such that $\forall\, t \geq T$ the stopping condition in (28) is met freezing the weighted posture error in vicinity ϵ.

Effectiveness of the terminal vehicle-straightening process strongly depends on the domination effect determined by (60). In the approximated case (for $\epsilon > 0$) final straightening precision is represented by a value of bound δ. More strictly, in the approximated case effectiveness of convergence (34) depends on how long the interval $T - t_D$ is. Obviously, the larger the difference $T - t_D$, the smaller terminal values of angles $\beta_{id}(t)$ (and, consequently, $\beta_i(t)$) can be obtained. Since the domination effect strongly depends on the difference $k_p - \eta$ and on the initial condition $\bar{\boldsymbol{e}}(0)$ (due to inherent properties of the VFO controller applied in the outer loop, see [9], [11]), hence the final straightening precision determined by δ is not only a function of vicinity ϵ and initial condition $\boldsymbol{\beta}(0)$, but also of difference $k_p - \eta$ and initial posture $\bar{\boldsymbol{e}}(0)$. Indeed, all the arguments of function $\delta(\epsilon, \bar{\boldsymbol{e}}(0), \boldsymbol{\beta}(0), k_p - \eta)$ determine how long the domination effect influences the vehicle motion allowing the vehicle chain to keep straightening before the stopping condition in (28) is activated. The above reasoning explains restrictions imposed on initial posture $\bar{\boldsymbol{e}}(0)$ in assumption A2.

Remark 2: According to definition (18) one observes that assumption A1 is met, when the product determined by (17) is positive for any i, i.e. when velocities v_{id} have a common sign for $i = 0, \dots, N$. Potential violation of A1 may occur especially if the guidance segment is initially too close to a reference position and the extensive reconfigurations of a vehicle chain are required[3]. In order to minimize the violation risk of A1 we propose to replace (15) by

$$v_{i-1d}(t) \triangleq \sigma \left| L_i \omega_{id}(t) \sin\beta_i(t) + v_{id}(t)\cos\beta_i(t) \right|, \quad (35)$$

where σ is a decision factor inherited from the VFO control strategy. Because of specific properties of the VFO control law $\operatorname{sgn}(\Phi_v(t)) = \sigma$ for definite fraction of a control duration [11]. Thus, by applying (35) instead of (15) makes it possible to confine (17) to set $\mathbb{R}_+$ for almost all $t \geq 0$, limiting in this way desired angle (18) to the first and fourth quadrants.

Remark 3: Dynamics of the i-th joint-angle error result from equation $\dot{e}_{id} = -k_i e_{id} + \sum_{j=1}^{i} \gamma_{ij} \sin e_{jd}$ (cf. (30)). To obtain a reasonable control quality in the i-th inner loop, convergence of $e_{jd}(t)$ for $j = 1, \dots, i-1$ should overtake convergence of $e_{id}(t)$. Since (54) determines the smallest required gain for JCM$_i$ modules, hence we propose to select:

$$k_1 > k_2 > k_3 > \ldots > k_N \quad \text{with} \quad k_N = \underline{k}. \quad (36)$$

For the outer-loop controller we propose to take :

$$k_a := 2k_p, \quad k_p > 0, \quad \eta \in (0, k_p). \quad (37)$$

The first rule is motivated by the VFO strategy, while the next two result from stability conditions of the VFO control system [11]. Practical selection of k_p should be a compromise between the convergence rate of error $\bar{\boldsymbol{e}}(t)$ and the resultant outer-loop sensitivity to measurement noises in the loop. Selection of η determines a desired intensity of the directing effect – the less the difference $k_p - \eta$, the higher intensity.

[3]This additionally justifies restrictions imposed on $\bar{\boldsymbol{e}}(0)$ in assumption A2.

E. Comments on control implementation

Terms $\dot{\beta}_{id}$ in (19) may be obtained by formal differentiation of (18) requiring time-derivatives of signals ω_{id} and v_{id}. Since it may cause some difficulties in practice, one may estimate $\dot{\beta}_{id}$ by using the concept of exact differentiator (see [17]). Moreover, in a case of slow vehicle motion implementation of terms $\dot{\beta}_{id}$ can be omitted.

In practice, one should take into account control-input limitations resulting from the maximal admissible wheel velocity $\omega_m > 0$ of a tractor. Let us recall a simple scaling procedure which allows addressing these limitations [9], [11]. Desired velocities for the tractor wheels result from the formula

$$\boldsymbol{\omega}_d = \begin{bmatrix} \omega_{Rd} \\ \omega_{Ld} \end{bmatrix} = \boldsymbol{P}^{-1}\boldsymbol{u}_{0d}, \qquad \boldsymbol{P} = \begin{bmatrix} r_w/b & -r_w/b \\ r_w/2 & r_w/2 \end{bmatrix}, \quad (38)$$

where r_w and b are a wheel radius and a wheel base of the tractor, respectively, and $\boldsymbol{u}_{0d} = [\omega_{0d} \; v_{0d}]^\top$ is the control vector computed according to (20). Now, input limitations can be respected by application of the rescaled control

$$\boldsymbol{u}_0 := \frac{\boldsymbol{u}_{0d}}{s}, \quad s \triangleq \max\left\{1; \frac{|\omega_{Rd}(t)|}{\omega_m}; \frac{|\omega_{Ld}(t)|}{\omega_m}\right\} \geq 1. \quad (39)$$

Control (39) is feasible and preserves the desired instantaneous motion curvature of the tractor determined by $\boldsymbol{u}_{0d}$ (cf. [11]).

IV. Numerical validation

Simulations have been carried out for S3T kinematics using $L_i = 0.229\,\text{m}$, $i = 1, 2, 3$. Three examples SA, SB, and SC have been considered using the following common parameters: $k_1 = 60$, $k_2 = 40$, $k_3 = 10$, $k_a = 2$, $k_p = 1$, $\eta = 0.8$. Example SA has been conducted taking $\epsilon = 0$ (nominal case) and using modification (35), while SB and SC have been conducted for $\epsilon = 0.005$, $w_\theta = 1$, and using definition (15). The term $\dot{\beta}_{1d}$ has been implemented by filtered numerical differentiation of β_{1d}, while $\dot{\beta}_{id}$ for $i = 2, 3$ have been omitted. Scaling procedure (38)-(39) has been implemented assuming $\omega_m = 8\pi$ rad/s, $r_w = 0.025\,\text{m}$ and $b = 0.17\,\text{m}$. The following reference postures and motion strategies have been selected: $\bar{\boldsymbol{q}}_r = [\frac{\pi}{2} \; -1 \; 0]^\top$ and $\sigma = -1$ for SA, $\bar{\boldsymbol{q}}_r = [-\frac{\pi}{2} \; -1 \; -1]^\top$ and $\sigma = -1$ for SB, $\bar{\boldsymbol{q}}_r = [0 \; 1 \; 1]^\top$ and $\sigma = +1$ for SC.

The results presented in Fig. 3 show the non-oscillatory motion of the guidance segment with the directing effect represented by specific approaching strategy to the reference posture. Control signals do not exceed the maximal feasible values within the whole control time-horizon. Terminal oscillations of desired angle $\beta_{1d}(t)$ (and, as a consequence, of signals $\omega_0(t)$ and $\beta_1(t)$) in the case of simulation SA are caused by increasing numerical sensitivity of functions $\text{Atan2c}\,(\cdot,\cdot)$ when both their arguments become very close to zero (a well known property of function $\text{Atan2c}\,(\cdot,\cdot)$). Terminal oscillations have been efficiently avoided in simulations SB and SC by introducing $\epsilon > 0$ (with a cost of slightly deteriorated final precision of docking). Simulation SA is an example where substantial initial reconfigurations of a vehicle chain were required. Therefore in these conditions application of modification (35) was necessary (in the opposite case assumption A1 would be permanently violated and $\beta_{3d}(t)$ would converge toward $-\pi$). On the other hand, note that temporary initial violation of A1 by angle β_{3d} has not destroyed boundedness and convergence of any signal in the closed-loop system; it portrays A1 as a slightly conservative assumption.

V. Experimental verification

Figure 4 presents the 3-trailer experimental RMP vehicle. The last trailer of a vehicle is equipped with a LED marker which allows estimating posture $\bar{\boldsymbol{q}}$ by an external vision system. Kinematic parameters of the RMP vehicle are as follows: $L_i = 0.229\,\text{m}$, $i = 1, 2, 3$, $r_w = 0.02925\,\text{m}$, $b = 0.15\,\text{m}$.

Two experiments, EA and EB, have been conducted using the parameters: $k_1 = 60$, $k_2 = 40$, $k_3 = 10$, $k_a = 2$, $k_p = 1$, $\eta = 0.6$, $\sigma = -1$, $\epsilon = 0.02$, $w_\theta = \sqrt{0.001}$, $\omega_m = 3\,\text{rad/s}$. In both experiments: terms $\dot{\beta}_{id}$ have been omitted in implementation, definition (35) has been used, and reference posture $\bar{\boldsymbol{q}}_r = \boldsymbol{0}$ has been selected. Pushing control $\phi_v(\bar{\boldsymbol{e}})$ of the VFO controller has been modified to a more general form $\Phi_v(\bar{\boldsymbol{e}}) = \xi(\bar{\boldsymbol{e}}) \cdot (h_x \cos\theta_N + h_y \sin\theta_N)$ with $\xi(\bar{\boldsymbol{e}}) = (e_x^2 + e_y^2)^{\alpha/2}/(h_x^2 + h_y^2)^{1/2}$ taking $\alpha = 0.4$. This modification prevents very sluggish terminal motion of the guidance segment. Experimental results in Fig. 5 generally show that terminal quality of the vehicle-chain straightening is visibly deteriorated when compared to quality anticipated by simulations. This is a result of non-modeled mechanical nonidealities and measurement noises present in the feedback loops (especially in the outer loop). However, in both experiments the docking task has been successfully completed.

VI. Final remarks

A. Relating the proposed control law to existing solutions

The most celebrated approach to control of SNT vehicles available in the literature (called hereafter the *chained control*) requires auxiliary transformation of vehicle kinematics into the chained form [24], [27] (see also [34]), which is valid only locally for $|\beta_i| < \frac{\pi}{2}$, $i = 1, \ldots, N$, and $|\theta_N| \neq \frac{\pi}{2}$ (cf. [23], [27], [28]) or $|e_\theta| < \frac{\pi}{2}$ (cf. [31]). Satisfaction of the above restrictions allows one to utilize one of the numerous stabilizers devised for the chained-form model, see e.g. [3], [4], [20], [22], [23], [32]. Application of the cascaded VFO controller does not require any auxiliary transformation, hence it does not suffer from configuration restrictions characteristic for chained control[4]. Formulation of the cascaded controller in the original configuration space makes its structure clearly interpretable. As a consequence, controller tuning is simple and invariant to initial vehicle configurations. In contrast, difficulties with controller tuning and substantial closed-loop

[4]Worth to note that assumption A1 concerns angles β_{id}, not β_i.

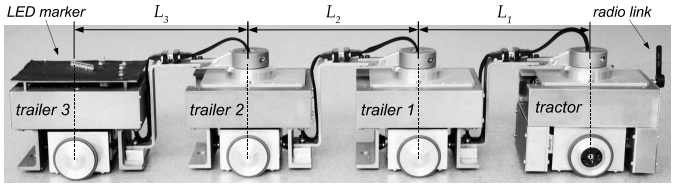

Fig. 4. RMP 3-trailer vehicle used in experiments

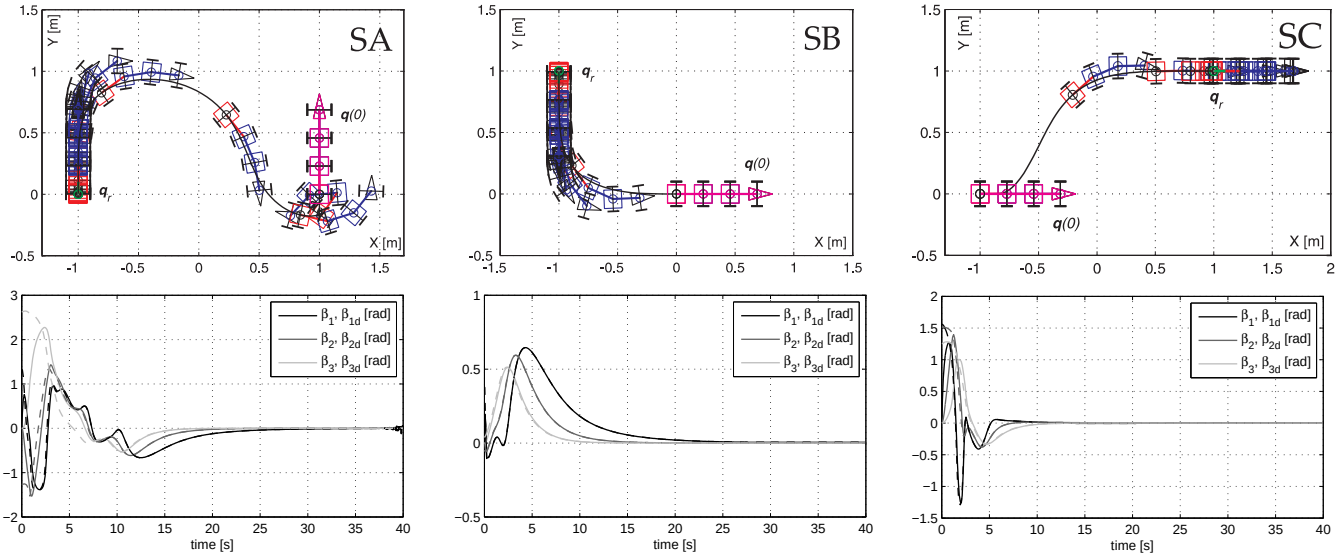

Fig. 3. Results of simulations SA, SB, and SC. Initial $\boldsymbol{q}(0)$ and reference $\boldsymbol{q}_r$ configurations have been denoted on the X-Y plots together with a path drawn by a guidance point located on the last trailer (the segment highlighted in red). Evolution of desired joint-angles β_{id} have been denoted by dashed lines

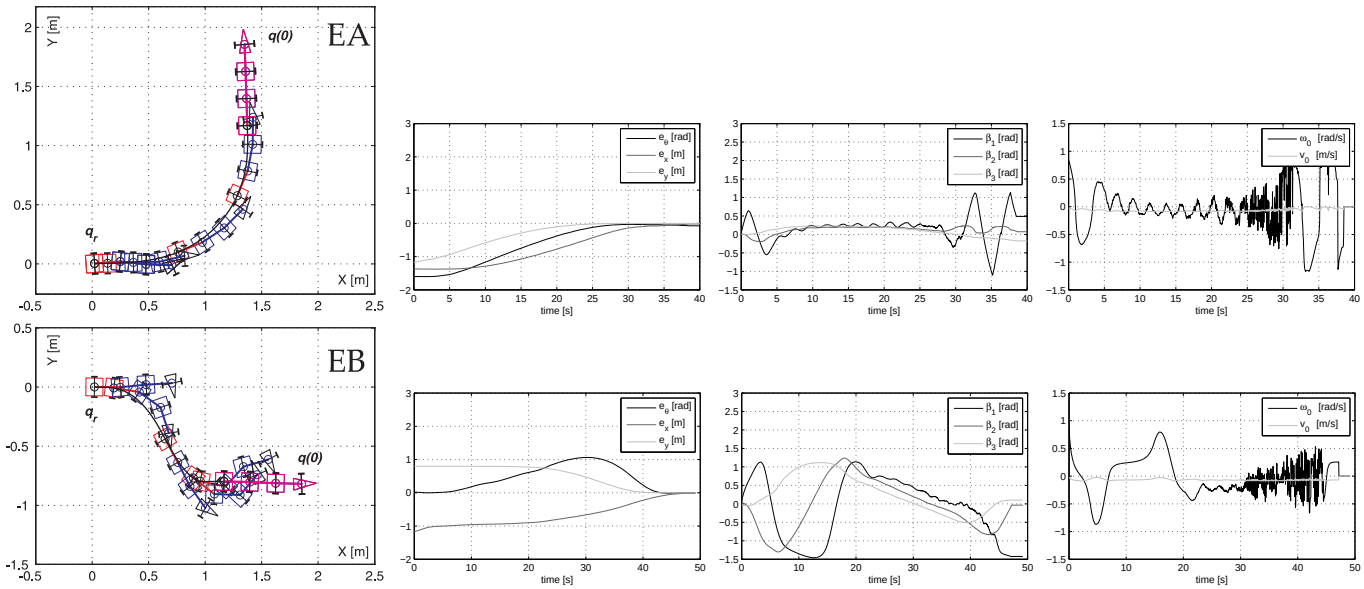

Fig. 5. Results of experiments EA and EB. Initial $\boldsymbol{q}(0)$ and reference $\boldsymbol{q}_r$ configurations have been denoted on the X-Y plots together with a path drawn by a guidance point located on the last trailer (the segment highlighted in red)

sensitivity have been revealed in [21] and [26] in the context of chained controllers. In practice, in order to preserve acceptable control performance in the task space with a change of the vehicle initial configuration manual re-tuning of the chained controller parameters is often required. Similar difficulties with relation to the fuzzy-controller have been reported in [29].

The next important issue concerns scalability of a controller. In the cascaded approach a change in a number of trailers affects only a number of JCM blocks in the inner loop retaining complexity of the controller virtually unchanged. In contrast, complexity of chained and fuzzy controllers largely depends on a number of trailers (cf. [26] and [29], [33]).

Finally, let us address the issue of control performance. Figure 6 illustrates the results of exemplary comparative simulations conducted for S2T kinematics, assuming $\bar{\boldsymbol{q}}_r = \mathbf{0}$ and prescribing $\boldsymbol{q}(0) = [\beta_1(0)\ \beta_2(0)\ \theta_2(0)\ x_2(0)\ y_2(0)]^\top = [\mathbf{0}_{1\times 3}\ 1\ 0.3]^\top$, by using the proposed controller (denoted as VFO) and three alternative chained controllers: continuous time-varying (CTV) stabilizer proposed in [22], discontinuous time-varying (DTV called also *hybrid*) stabilizer presented in [32], and discontinuous time-invariant (DVI) stabilizer developed in [3]. The results in Fig. 6 show essential difference in control performance obtained with the time-varying and time-invariant stabilizers. Time-dependent stabilization usually characterizes by highly oscillatory control with possible substantial transient departures from the set-point (cf. CTV and DTV cases in Fig. 6). Time-invariant stabilizers ensure non-oscillatory behavior of the guidance segment. This difference is also visible on the logarithmic plot of $\|\boldsymbol{q}(t)\|$, where one may observe the exponential convergence rate for all the

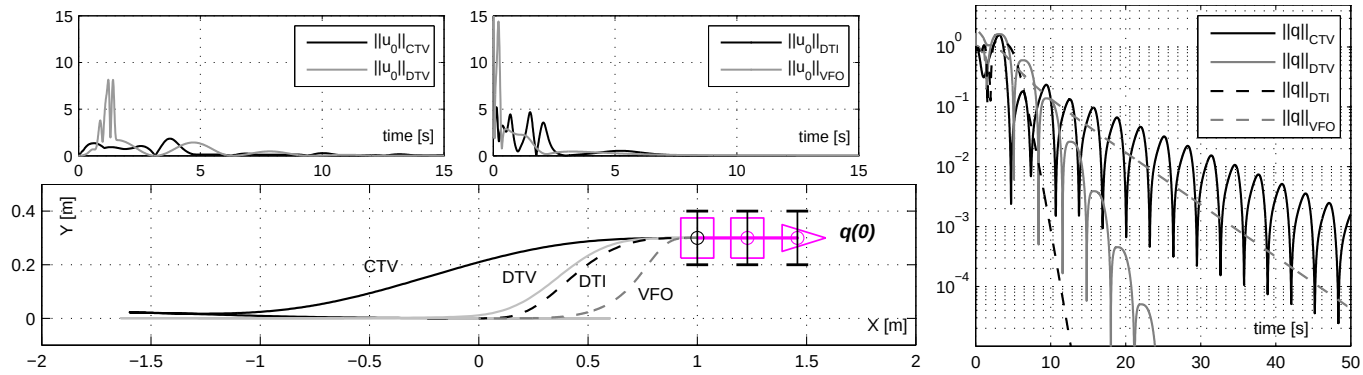

Fig. 6. Comparison of shifted-parallel parking maneuvers to the zero reference configuration achieved by the proposed cascaded controller (VFO) and three alternative set-point chained controllers (CTV, DTV, and DTI) for S2T kinematics (initial vehicle configuration $\boldsymbol{q}(0)$ has been denoted on the X-Y plot)

compared algorithms. On the other hand, CTV and DTV controllers are 'true stabilizers' which asymptotically stabilize all the configuration variables. In contrast, DTI controller ensures only convergence of state variables if $x_2(0) \neq 0$, cf. [3]. The VFO controller appears as an intermediate solution, which guarantees asymptotic stabilization of posture $\bar{\boldsymbol{q}}$ (if $\epsilon = 0$), but assures only convergence of angles $\beta_i(t)$. In this context, considered DTI and VFO controllers are not able to make the joint angles converge in the special case when $\bar{\boldsymbol{e}}(0) = \mathbf{0}$ and $\boldsymbol{\beta}(0) \neq \mathbf{0}$, while CTV and DTV controllers can do that. For initial conditions presented in Fig. 6 performance achieved with DTI and VFO stabilizers looks similar. The higher initial control cost is observed for VFO controller (with $\| \boldsymbol{u}_0(0)\|_{\text{VFO}} \approx 50$ not shown for clarity of the plot), which however leads to a more smooth behavior of the vehicle chain in the later control stage. Smoothness of the guidance segment motion and vehicle motion strategy (forward/backward) can be easily modified in the VFO approach by parameter η and decision factor σ, respectively, while similar influence of the DTI controller parameters is not completely clear.

B. Conclusions

Solution to the set-point control problem for N-trailers with on-axle hitching has been presented by using the cascaded control approach with application of the VFO outer-loop controller. The control law proposed in the paper does not require any auxiliary transformation of a vehicle model, and provides a highly scalable solution for vehicles with an arbitrary number of trailers. Because of the simple cascaded control structure particular control components have clear functional interpretation, which makes a tuning process of the controller especially simple. Revealed noise-sensitivity of the closed-loop system, increasing in a terminal control stage, can be relaxed in practice by prescribing larger vicinity ϵ.

APPENDIX A

Angle $\varphi(t) = \text{Atan2c}\,(b_1(t), b_2(t))$ is equivalent to time-integral $\varphi(t) = \int_0^t \frac{\dot{b}_1(\xi)b_2(\xi) - \dot{b}_2(\xi)b_1(\xi)}{b_1^2(\xi)+b_2^2(\xi)} d\xi$. For the discrete-time domain an alternative computational algorithm is provided below. Let $b_1(n)$ and $b_2(n)$ denote two real-valued arguments determined in the discrete time $n \in \mathbb{N}$. Angle $\varphi(n) = \text{Atan2c}\,(b_1(n), b_2(n))$ can be obtained in five steps:

S1. $\Phi(n) = \text{Atan2}\,(b_1(n), b_2(n)) \in (-\pi, \pi]$

S2. $\Phi(n-1) = \text{Atan2}\,(\sin\varphi(n-1), \cos\varphi(n-1)) \in (-\pi, \pi]$

S3. $\Delta\Phi(n) = \Phi(n) - \Phi(n-1)$

S4. IF $\Delta\Phi(n) > +\pi$ THEN $\Delta\varphi(n) = \Delta\Phi(n) - 2\pi$
ELSEIF $\Delta\Phi(n) < -\pi$ THEN $\Delta\varphi(n) = \Delta\Phi(n) + 2\pi$
ELSE $\Delta\varphi(n) = \Delta\Phi(n)$

S5. $\varphi(n) = \varphi(n-1) + \Delta\varphi(n) \quad \Rightarrow \quad \varphi(n) \in \mathbb{R}$

where $\varphi(n-1)$ is an angle value from the previous time instant which has to be stored in a memory.

APPENDIX B

Inequality in A1 implies $B_{id} \triangleq \sup_{t\geq 0} |\tan\beta_{id}(t)| < \infty$ for $i = 1, \ldots, N$. According to (14) and G1 in Lemma 1 $|\omega_{Nd}| \leq \Omega_{Nd} < \infty$ and $|v_{Nd}| \leq V_{Nd} < \infty$, where $\Omega_{Nd} = \sup_{t\geq 0} |\Phi_\omega(\bar{\boldsymbol{e}}(t))|, V_{Nd} = \sup_{t\geq 0} |\Phi_v(\bar{\boldsymbol{e}}(t))|$. Using (15) for $i = N$ we have $|v_{N-1d}| < (L_N\Omega_{Nd} + V_{Nd}) =: V_{N-1d} < \infty$. Recalling (16)-(18) we have $|\omega_{N-1d}| < \frac{V_{N-1d}B_{N-1d}}{L_{N-1}} =: \Omega_{N-1d} < \infty$, where we have used A1. Using (15) for $i = N-1$ we have $|v_{N-2d}| < (1 + B_{N-1d})(L_N\Omega_{Nd} + V_{Nd}) =: V_{N-2d} < \infty$. Recalling (16)-(18) one can write $|\omega_{N-2d}| < \frac{1}{L_{N-2}} V_{N-2d}B_{N-2d} =: \Omega_{N-2d} < \infty$. Hence, by using (15) for $i = N-2$ one can write $|v_{N-3d}| < (1 + B_{N-2d})(1 + B_{N-1d})(L_N\Omega_{Nd} + V_{Nd}) =: V_{N-3d} < \infty$, etc. Proceeding the similar reasoning by decreasing index i we have $\sup_{t\geq 0} |v_{N-id}(t)| < V_{N-id}$ for $i = 0, \ldots, N$ using

$$V_{Nd} = \sup_{t\geq 0} |\Phi_v(\bar{\boldsymbol{e}}(t))|, \quad \Omega_{Nd} = \sup_{t\geq 0} |\Phi_\omega(\bar{\boldsymbol{e}}(t))|, \tag{40}$$

$$V_{N-1d} = (L_N\Omega_{Nd} + V_{Nd}), \tag{41}$$

$$V_{N-id} = (L_N\Omega_{Nd} + V_{Nd}) \prod_{j=1}^{i-1} (1 + B_{N-jd}), \tag{42}$$

where (42) applies for $i = 2, \ldots, N$. Under assumption A1 the bounds determined by (42) are finite. An alternative form of upper bound (42) can be formulated by substituting $i := N - i$

$$V_{id} = (L_N\Omega_{Nd} + V_{Nd}) \prod_{j=1}^{N-i-1} (1 + B_{N-jd}), \tag{43}$$

which is valid now for $i = 0, \ldots, N-2$.

APPENDIX C

Inequality in assumption A1 allows defining the bound

$$C_{id} \triangleq \inf_{t\geq 0} |\cos\beta_{id}(t)| > 0, \tag{44}$$

which will be used in the proofs below.

a) Proof of Lemma2: Let us introduce the errors:

$$\boldsymbol{e}_{\omega v} \triangleq \begin{bmatrix}\boldsymbol{e}_\omega \\ \boldsymbol{e}_v\end{bmatrix},\ \boldsymbol{e}_\omega \triangleq \begin{bmatrix}\omega_{1d}-\omega_1 \\ \vdots \\ \omega_{Nd}-\omega_N\end{bmatrix},\ \boldsymbol{e}_v \triangleq \begin{bmatrix}v_{1d}-v_1 \\ \vdots \\ v_{Nd}-v_N\end{bmatrix}. \tag{45}$$

Differentiating (11) with respect to time, then using (12) and (19) allows one to write: $\dot{e}_{id} = \dot{\beta}_{id} - \dot{\beta}_i = \dot{\beta}_{id} - \omega_{i-1} + \omega_i + \omega_{i-1d} - \omega_{i-1d} = \dot{\beta}_{id} - \omega_{i-1} + \omega_i + \omega_{i-1d} - (k_i e_{id} + \dot{\beta}_{id} + \omega_{id}) = -k_i e_{id} + (\omega_{i-1d} - \omega_{i-1}) - (\omega_{id} - \omega_i)$. Combining the above equations for $i = 1, \ldots, N$ gives the linear perturbed dynamics

$$\dot{\boldsymbol{e}}_d = -\boldsymbol{A}\boldsymbol{e}_d + \boldsymbol{\Lambda}\boldsymbol{e}_\omega, \tag{46}$$

with $\boldsymbol{A} = \text{diag}\{k_1, k_2, \ldots, k_N\}$, and

$$\boldsymbol{\Lambda}_{N\times N} = \begin{bmatrix}-1 & 0 & \ldots & 0 \\ 1 & -1 & \ldots & 0 \\ \vdots & \vdots & \ddots & \vdots \\ 0 & 0 & \ldots & -1\end{bmatrix}. \tag{47}$$

It can be shown that

$$\boldsymbol{e}_\omega = \boldsymbol{W}\sin\boldsymbol{e}_d, \tag{48}$$

where $\sin\boldsymbol{e}_d \triangleq \begin{bmatrix}\sin e_{1d} & \ldots & \sin e_{Nd}\end{bmatrix}^\top \in [-1,1]^N$, and $\boldsymbol{W}_{N\times N}$ is a lower-triangular matrix with the diagonal elements $w_{ii} = \frac{\cos\beta_i}{L_i\cos\beta_{id}} v_{id}$, and with the non-zero off-diagonal elements $w_{il} = -\frac{\sin\beta_i}{L_i}\sum_{j=1}^{l} \frac{v_{jd}\sin\beta_j \prod_{k=j+1}^{l}\cos\beta_k}{\cos\beta_{jd}}$ for $i = 2, \ldots, N$ and $l = 1, \ldots, i-1$. Using bounds (44) and (40)-(43) one observes that all elements of $\boldsymbol{W}$ are bounded satisfying ($i = 1, \ldots, N$, $l = 1, \ldots, i-1$):

$$|w_{ii}| < \frac{V_{id}}{L_i C_{id}} < \infty, \qquad |w_{il}| < \frac{1}{L_i}\sum_{j=1}^{l}\frac{V_{jd}}{C_{jd}} < \infty. \tag{49}$$

Applying (48) into (46) yields the equation

$$\dot{\boldsymbol{e}}_d = -\boldsymbol{A}\boldsymbol{e}_d + \boldsymbol{\Gamma}\sin\boldsymbol{e}_d, \tag{50}$$

with the lower-triangular matrix $\boldsymbol{\Gamma} = \boldsymbol{\Lambda}\boldsymbol{W} = [\gamma_{ij}]$, $i, j \in \{1, \ldots, N\}$, where the non-zero elements have the forms:

$$\begin{array}{ll}\gamma_{ii} & = -w_{ii} \quad \text{for } i = 1, \ldots, N \\ \gamma_{ij} & = w_{i-1,j} - w_{ij} \quad \text{for } j < i\end{array}. \tag{51}$$

According to (51) and (49) all the elements of matrix $\boldsymbol{\Gamma}$ are bounded. As a consequence

$$\|\boldsymbol{\Gamma}\| \leq N\|\boldsymbol{\Gamma}\|_{\max} = N\max_{i,j}|\gamma_{ij}| \leq g, \tag{52}$$

where $g \in (0, \infty)$, and $\|\boldsymbol{\Gamma}\|_{\max} \triangleq \max_{i,j}|\gamma_{ij}|$.

Taking the positive definite function $V_{e_d}(\boldsymbol{e}_d) \triangleq \frac{1}{2}\boldsymbol{e}_d^\top\boldsymbol{e}_d$, its time-derivative can be estimated as follows:

$$\begin{aligned}\dot{V}_{e_d} &= \boldsymbol{e}_d^\top\dot{\boldsymbol{e}}_d \overset{(50)}{=} \boldsymbol{e}_d^\top(-\boldsymbol{A}\boldsymbol{e}_d + \boldsymbol{\Gamma}\sin\boldsymbol{e}_d) \\ &\leq -\underline{\lambda}_{\boldsymbol{A}}\|\boldsymbol{e}_d\|^2 + \|\boldsymbol{\Gamma}\|\,\|\boldsymbol{e}_d\|^2 + \rho\underline{\lambda}_{\boldsymbol{A}}\|\boldsymbol{e}_d\|^2 - \rho\underline{\lambda}_{\boldsymbol{A}}\|\boldsymbol{e}_d\|^2 \\ &\leq -\underline{k}(1-\rho)\|\boldsymbol{e}_d\|^2 + (g - \rho\underline{k})\|\boldsymbol{e}_d\|^2,\end{aligned} \tag{53}$$

where we have used inequality (52), $\underline{\lambda}_{\boldsymbol{A}} = \underline{k} \triangleq \min_i\{k_i\}$ is a minimal eigenvalue of matrix $\boldsymbol{A}$, and $\rho \in (0,1)$. If one selects

$$\underline{k} \triangleq \min_i\{k_i\} \geq g/\rho, \tag{54}$$

then (53) satisfies: $\dot{V}_{e_d}(\boldsymbol{e}_d) \leq -2\underline{k}(1-\rho)V(\boldsymbol{e}_d)$. Since, the right-hand side is negative definite, thus: $\|\boldsymbol{e}_d(t)\| < \infty$ and $\|\boldsymbol{e}_d(t)\| \leq \|\boldsymbol{e}_d(0)\|\exp(-(1-\rho)\underline{k}t)$ for all $t \geq 0$.

b) Proof of Lemma3: For $\bar{\boldsymbol{q}}_r = \boldsymbol{0}$ the zero-input part of (33) corresponds to dynamics (27). Upon Lemma 1 and the comments afterwards in Section III-B, one observes that the zero-input part of (33) has the globally asymptotically stable equilibrium $\bar{\boldsymbol{e}} = \boldsymbol{0}$ (G1 to G3 in Lemma 1 are valid for any bounded $\bar{\boldsymbol{e}}(0)$). Upon the converse Lyapunov theorem (cf. [12], Th. 10.1.4) there exists a continuously differentiable function $V_{\bar{e}}(\bar{\boldsymbol{e}})$, and class $\mathcal{K}_\infty$ functions α_1, α_2, and α_3 such that:

$$\begin{aligned}&\alpha_1(\|\bar{\boldsymbol{e}}\|) \leq V_{\bar{e}}(\bar{\boldsymbol{e}}) \leq \alpha_2(\|\bar{\boldsymbol{e}}\|) \qquad \text{for all } \|\bar{\boldsymbol{e}}\| < \infty, \\ &\frac{\partial V_{\bar{e}}(\bar{\boldsymbol{e}})}{\partial\bar{\boldsymbol{e}}}\boldsymbol{f}_n(\bar{\boldsymbol{e}}) \leq -\alpha_3(\|\bar{\boldsymbol{e}}\|) \qquad \text{for all } \|\bar{\boldsymbol{e}}\| < \infty.\end{aligned}$$

From the fact that $V_{\bar{e}}$ is continuously differentiable it must be $\left|\dot{V}_{\bar{e}}\right| = \left|\frac{\partial V_{\bar{e}}(\bar{\boldsymbol{e}})}{\partial\bar{\boldsymbol{e}}}\boldsymbol{f}_n(\bar{\boldsymbol{e}})\right| < \infty$. Since $\|\boldsymbol{f}_n(\bar{\boldsymbol{e}})\| = \left\|\bar{\boldsymbol{G}}(-\bar{\boldsymbol{e}})\boldsymbol{\Phi}(\bar{\boldsymbol{e}})\right\| \leq \|\boldsymbol{\Phi}(\bar{\boldsymbol{e}})\| < \infty$ (cf. (27) and G1 in Lemma 1), we must have for some positive $\alpha \in (0, \infty)$

$$\left\|\frac{\partial V_{\bar{e}}(\bar{\boldsymbol{e}})}{\partial\bar{\boldsymbol{e}}}\right\| \leq \alpha \qquad \text{for all } \|\bar{\boldsymbol{e}}\| < \infty. \tag{55}$$

In the context of dynamics (33), it can be shown that

$$\boldsymbol{e}_{\omega v} = \begin{bmatrix}\boldsymbol{e}_\omega \\ \boldsymbol{e}_v\end{bmatrix} = \begin{bmatrix}\boldsymbol{W}\sin\boldsymbol{e}_d \\ \boldsymbol{V}\sin\boldsymbol{e}_d\end{bmatrix} = \boldsymbol{H}\sin\boldsymbol{e}_d, \tag{56}$$

where the first component has been introduced in (48), while $\boldsymbol{V}_{N\times N}$ is a lower-triangular matrix with diagonal elements in the form $\nu_{ii} = -\frac{\sin\beta_i}{\cos\beta_{id}}v_{id}$, and the non-zero off-diagonal elements $\nu_{il} = -\sum_{j=1}^{l}\frac{v_{jd}\sin\beta_j\prod_{k=j+1}^{l+1}\cos\beta_k}{\cos\beta_{jd}}$ for $i = 2, \ldots, N$ and $l = 1, \ldots, i-1$. Using bounds (44) and (40)-(43) one can observe that absolute values of all the elements of matrix $\boldsymbol{V}$ are bounded from above satisfying ($i = 1, \ldots, N$, $l = 1, \ldots, i-1$): $|\nu_{ii}| < \frac{V_{id}}{C_{id}}$, $|\nu_{il}| < \sum_{j=1}^{l}\frac{V_{jd}}{C_{jd}}$. As a consequence, $\|\boldsymbol{V}\| \leq N\|\boldsymbol{V}\|_{\max} = N\max_{i,j}|\nu_{ij}| \leq g_V$, where $g_V \in (0, \infty)$, and $\|\boldsymbol{V}\|_{\max} \triangleq \max_{i,j}|\nu_{ij}|$. By analogy, and using (49), holds: $\|\boldsymbol{W}\| \leq N\|\boldsymbol{W}\|_{\max} = N\max_{i,j}|w_{ij}| \leq g_W$ with $g_W \in (0, \infty)$. Hence, by recalling (56), one can assess a bound of the perturbing term introduced in (33) as:

$$\|g(\bar{\boldsymbol{e}}, \boldsymbol{e}_d)\| \leq \left\|\bar{\boldsymbol{G}}(-\bar{\boldsymbol{e}})\right\|\|\boldsymbol{L}\boldsymbol{H}\|\,\|\sin\boldsymbol{e}_d\| \leq \bar{\gamma}\,\|\boldsymbol{e}_d\|, \tag{57}$$

where $\bar{\gamma} = (g_W + g_V)$ is a finite positive constant.

Now, let us assess the time-derivative of $V_{\bar{e}}$ for original system (33) with $\boldsymbol{e}_d$ viewed as an input:

$$\begin{aligned}\dot{V}_{\bar{e}} &= \frac{\partial V_{\bar{e}}(\bar{\boldsymbol{e}})}{\partial\bar{\boldsymbol{e}}}\boldsymbol{f}(\bar{\boldsymbol{e}}, \boldsymbol{e}_d) = \frac{\partial V_{\bar{e}}(\bar{\boldsymbol{e}})}{\partial\bar{\boldsymbol{e}}}\boldsymbol{f}_n(\bar{\boldsymbol{e}}) + \frac{\partial V_{\bar{e}}(\bar{\boldsymbol{e}})}{\partial\bar{\boldsymbol{e}}}\boldsymbol{g}(\bar{\boldsymbol{e}}, \boldsymbol{e}_d) \\ &\leq -\alpha_3(\|\bar{\boldsymbol{e}}\|) + \alpha\bar{\gamma}\,\|\boldsymbol{e}_d\| \leq -\bar{\alpha}_3(\|\bar{\boldsymbol{e}}\|) + \alpha\bar{\gamma}\,\|\boldsymbol{e}_d\| \\ &= -(1-\gamma)\bar{\alpha}_3(\|\bar{\boldsymbol{e}}\|) + \alpha\bar{\gamma}\,\|\boldsymbol{e}_d\| - \gamma\bar{\alpha}_3(\|\bar{\boldsymbol{e}}\|),\end{aligned} \tag{58}$$

with $\gamma \in (0,1)$, $\bar{\alpha}_3$ being a function of class $\mathcal{K}$, and where we have used (55) and (57). According to (58) one concludes

$$\dot{V}_{\bar{e}} \leq -(1-\gamma)\bar{\alpha}_3(\|\bar{\boldsymbol{e}}\|) \quad \text{for } \|\bar{\boldsymbol{e}}\| \geq \bar{\alpha}_3^{-1}\left(\frac{\alpha\bar{\gamma}}{\gamma}\|\boldsymbol{e}_d\|\right).$$

Using Th. 4.19 presented in [15], system (33) is ISS with respect to $\boldsymbol{e}_d$. Hence, upon Th. 10.4.5 formulated in [12] holds

$$\limsup_{t\to\infty} \| \bar{\boldsymbol{e}}(t)\| \leq \chi(\limsup_{t\to\infty} \| \boldsymbol{e}_d(t)\|), \tag{59}$$

where $\chi(\cdot)$ is some function of class $\mathcal{K}$.

c) Proof of Lemma4: Combining G2 and G3 of Lemma 1 yields: $\Phi_\omega(\bar{\boldsymbol{e}}(t)), \Phi_v(\bar{\boldsymbol{e}}(t)) \to 0$ as $t \to \infty$. However, because of the directing effect which is characteristic for the VFO control strategy, the following *terminal domination property* holds [9], [11]: $F_D(t) \overset{t\to\infty}{\longrightarrow} 0$ where $F_D(t) \triangleq |\Phi_\omega(\bar{\boldsymbol{e}}(t))| \,/\, |\Phi_v(\bar{\boldsymbol{e}}(t))|$. Thus, one observes that feedback function $\Phi_v(\bar{\boldsymbol{e}}(t))$ terminally dominates over $\Phi_\omega(\bar{\boldsymbol{e}}(t))$. More strictly, the domination begins at some finite $t_D \geq 0$ where

$$F_D(t) < 1 \quad \text{for} \quad t \geq t_D. \tag{60}$$

The key factor affecting the domination is parameter η of the VFO controller – less difference $k_p - \eta$ implies smaller t_D.

Using the above domination property and recalling (15) for $i = N$ one can observe that for $t \gg t_D$ hold (we use shortened notation $\mathrm{s}a \equiv \sin a$, $\mathrm{c}a \equiv \cos a$): $\omega_{Nd}(t) = \Phi_\omega(\bar{\boldsymbol{e}}(t)) \approx 0$ and $v_{N-1d}(t) \approx \Phi_v(\bar{\boldsymbol{e}}(t))\mathrm{c}\beta_N(t)$. Thus, according to (16)-(18) one observes that for $t \gg t_D$ $\beta_{Nd}(t) \to \text{Atan2c}\left(0, \Phi_v^2(\bar{\boldsymbol{e}}(t))\mathrm{c}\beta_N(t)\right) = 0$. The latter equality stems from the fact that $\Phi_v^2(\bar{\boldsymbol{e}}(t))\mathrm{c}\beta_N(t)$ will be positive when $e_{Nd}(t) \approx 0$ (cf. (31)) under assumption A1. Hence, if terminally $\beta_{Nd}(t), \dot{\beta}_{Nd}(t) \to 0$ one obtains from (19) and (31) that $\omega_{N-1d}(t) \approx 0$ for $t \gg t_D$. Based on the above estimation and by recalling (15) for $i = N-1$ one can write $v_{N-2d}(t) \approx \Phi_v(\bar{\boldsymbol{e}}(t))\mathrm{c}\beta_N(t)\mathrm{c}\beta_{N-1}(t)$ for $t \gg t_D$. According to (16)-(18) one observes $\beta_{N-1d}(t) \to \text{Atan2c}\left(0, \Phi_v^2(\bar{\boldsymbol{e}}(t))\mathrm{c}^2\beta_N(t)\mathrm{c}\beta_{N-1}(t)\right) = 0$. The latter equality results from the fact that $\Phi_v^2(\bar{\boldsymbol{e}}(t))\mathrm{c}^2\beta_N(t)\mathrm{c}\beta_{N-1}(t)$ will be positive when $e_{Nd}(t) \approx 0$ and $e_{N-1d}(t) \approx 0$ (cf. (31)) under assumption A1. Hence, if terminally $\beta_{N-1d}(t), \dot{\beta}_{N-1d}(t) \to 0$ and $\omega_{N-1d}(t) \approx 0$ (as shown above) then one obtains, according to (19) and (31), that $\omega_{N-2d}(t) \approx 0$ for $t \gg t_D$. The reasoning can be continued for all the remaining angles β_{id} by decreasing index i.

REFERENCES

[1] C. Altafini. Some properties of the general n-trailer. *International Journal of Control*, 74(4):409–424, 2001.

[2] N. P. I. Aneke, H. Nijmeijer, and A. G. de Jager. Tracking control of second-order chained form systems by cascaded backstepping. *Int. J. Robust Nonlinear Control*, 13:95–115, 2003.

[3] A. Astolfi. Discontinuous control of nonholonomic systems. *Systems & Control Letters*, 27:37–45, 1996.

[4] M. K. Bennani and P. Rouchon. Robust stabilization of flat and chained systems. In *3rd Europ. Control Conf.*, pages 2642–2646, Roma, 1995.

[5] P. Bolzern, R. M. DeSantis, A. Locatelli, and D. Masciocchi. Path-tracking for articulated vehicles with off-axle hitching. *IEEE Trans. on Control Systems Technology*, 6(4):515–523, 1998.

[6] A. Chaillet and A. Loria. Uniform semiglobal practical asymptotic stability for non-autonomous cascaded systems and applications. *Automatica*, 44:337–347, 2008.

[7] J.-M. Coron. On the stabilization of some nonlinear control systems: results, tools, and applications. In F. H. Clarke and R. J. Stern, editors, *Nonlinear Analysis, Differential Equations and Control*, pages 307–367. Kluwer Academic Publishers, 1999.

[8] M. Michałek. Geometrically motivated set-point control strategy for the standard N-trailer vehicle. In *2011 IEEE Intelligent Vehicles Symposium*, pages 138–143, Baden-Baden, Germany, 2011.

[9] M. Michałek. Application of the VFO method to set-point control for the N-trailer vehicle with off-axle hitching. *International Journal of Control*, 85(5):502–521, 2012.

[10] M. Michałek. Non-minimum-phase property of N-trailer kinematics resulting from off-axle interconnections. *International Journal of Control*, 86(4):740–758, 2013.

[11] M. Michałek and K. Kozłowski. Vector-Field-Orientation feedback control method for a differentially driven vehicle. *IEEE Trans. on Control Syst. Technology*, 18(1):45–65, 2010.

[12] A. Isidori. *Nonlinear Control Systems II*. Springer, London, 1999.

[13] F. Jean. The car with N trailers: characterisation of the singular configurations. *Control, Opt. Calc. Variations*, 1:241–266, 1996.

[14] Z. Jiang and H. Nijmeijer. A recursive technique for tracking control of nonholonomic systems in chained form. *IEEE Trans. on Automatic Control*, 44(2):265–279, 1999.

[15] H. K. Khalil. *Nonlinear systems. 3-Ed.* Prentice-Hall, New Jersey, 2002.

[16] J. P. Laumond. Controllability of a multibody mobile robot. *IEEE Trans. on Robotics and Automation*, 9(6):755–763, 1993.

[17] A. Levant. Higher-order sliding modes, differentiation and output-feedback control. *Int. J. Control*, 76(9/10):924–941, 2003.

[18] S.-J. Li and W. Respondek. Flat outputs of two-input driftless control systems. *ESAIM: Control, Optim. Calc. Variations*, 18:774–798, 2012.

[19] D. A. Lizarraga, P. Morin, and C. Samson. Chained form approximation of a driftless system. Application to the exponential stabilization of the general N-trailer system. *Int. J. Control*, 74(16):1612–1629, 2001.

[20] R. McCloskey and R. M. Murray. Exponential stabilization of driftless nonlinear control systems via time-varying, homogeneous feedback. *IEEE Trans. on Automatic Control*, pages 614–628, 1997.

[21] R. T. M'Closkey and R. M. Murray. Experiments in exponential stabilization of a mobile robot towing a trailer. In *Proc. of the American Control Conference*, pages 988–993, Baltimore, USA, 1994.

[22] P. Morin and C. Samson. Control of nonlinear chained systems: form the Routh-Hurwitz stability criterion to time-varying exponential stabilizers. *IEEE Trans. on Automatic Control*, 45(1):141–146, 2000.

[23] P. Morin and C. Samson. Transverse function control of a class of non-invariant driftless systems. Application to vehicles with trailers. In *Proc. 47th IEEE Conf. Dec. and Control*, pages 4312–4319, Cancun, 2008.

[24] R. M. Murray and S. S. Sastry. Nonholonomic motion planning: steering using sinusoids. *IEEE Trans. on Aut. Control*, 38(5):700–716, 1993.

[25] W. Pasillas-Lepine and W. Respondek. Nilpotentization of the kinematics of the n-trailer system at singular points and motion planning through the singular locus. *Int. J. Control*, 74(6):628–637, 2001.

[26] D. Pazderski, K. Kozłowski, and D. Waśkowicz. Control of a unicycle-like robot with trailers using transverse function approach. *Bulletin of the Polish Academy of Sciences. Technical Sciences*, 60(3):537–546, 2012.

[27] O. J. Sørdalen. Conversion of the kinematics of a car with n trailers into a chained form. In *Proc. IEEE Int. Conf. on Robotics and Automation*, pages 382–387, Atlanta, USA, 1993.

[28] O. J. Sørdalen and K. Y. Wichlund. Exponential stabilization of a car with n trailers. In *Proceedings of the 32th Conference on Decision and Control*, pages 978–983, San Antonio, USA, 1993.

[29] A. Riid, J. Ketola, and E. Rüstern. Fuzzy knowledge-based control for backing multi-trailer systems. In *Proceedings of the 2007 IEEE Intell. Vehicles Symp.*, pages 498–504, Istambul, Turkey, 2007.

[30] P. Rouchon, M. Fliess, J. Levine, and P. Martin. Flatness, motion planning and trailer systems. In *Proceedings of the 32nd Conference on Decision and Control*, pages 2700–2705, San Antonio, Texas, 1993.

[31] C. Samson. Control of chained systems. Application to path following and time-varying point-stabilization of mobile robots. *IEEE Trans. on Automatic Control*, 40(1):64–77, 1995.

[32] O. J. Sørdalen and O. Egeland. Exponential stabilization of nonholonomic chained systems. *IEEE Trans. Aut. Control*, 40(1):35–49, 1995.

[33] K. Tanaka, S. Hori, and H. O. Wang. Multiobjective control of a vehicle with triple trailers. *IEEE Trans. on Mechatronics*, 7(3):357–368, 2002.

[34] D. Tilbury, R. M. Murray, and S. S. Sastry. Trajectory generation for the N-trailer problem using Goursat normal form. *IEEE Trans. on Automatic Control*, 40(5):802–819, 1995.

[35] D. Tilbury, O. J. Sørdalen, L. Bushnell, and S. S. Sastry. A multisteering trailer system: conversion into chained form using dynamic feedback. *IEEE Trans. on Robotics and Automation*, 11(6):807–818, 1995.

[36] K. Yoo and W. Chung. Pushing motion control of n passive off-hooked trailers by a car-like mobile robot. In *2010 IEEE int. Conf. Robotics and Automation*, pages 4928–4933, Anchorage, USA, 2010.